ISSN 1674-1056
http://cpb.iphy.ac.cn
http://iopscience.iop.org/cpb
中国物理 B
Chinese Physics
中国物理
Chinese Physics B

Design and optimization of microstructure optical fiber sensor based on bimetal plasmon mode interaction

Meng Wu(吴萌)[1,2,3], Xin-Yu Liu(刘欣宇)[1,2,3], Gui-Yao Zhou(周桂耀)[1,2,3], Chang-Ming Xia(夏长明)[1,2,3], Bo-Yao Li(李波瑶)[1,2,3], Zhi-Yun Hou(侯峙云)[1,2,3]

Citation: Chin. Phys. B . 2019, 28(12): 124202 . **doi:** 10.1088/1674-1056/ab4d48
Journal homepage: http://cpb.iphy.ac.cn; http://iopscience.iop.org/cpb

What follows is a list of articles you may be interested in

Numerical investigation on coherent mid-infrared supercontinuum generation in chalcogenide PCFs with near-zero flattened all-normal dispersion profiles

Jie Han(韩杰), Sheng-Dong Chang(常圣东), Yan-Jia Lyu(吕彦佳), Yong Liu(刘永)
Chin. Phys. B . 2019, 28(10): 104204 . **doi:** 10.1088/1674-1056/ab3f25

Refractive index sensor based on high-order surface plasmon resonance in gold nanofilm coated photonic crystal fiber

Zhen-Kai Fan(范振凯), Shao-Bo Fang(方少波), Shu-Guang Li(李曙光), Zhi-Yi Wei(魏志义)
Chin. Phys. B . 2019, 28(9): 094209 . **doi:** 10.1088/1674-1056/ab327a

Multiple Fano resonances in nanorod and nanoring hybrid nanostructures

Xijun Wu(吴希军), Ceng Dou(窦层), Wei Xu(徐伟), Guangbiao Zhang(张广彪), Ruiling Tian(田瑞玲), Hailong Liu(刘海龙)
Chin. Phys. B . 2019, 28(1): 014204 . **doi:** 10.1088/1674-1056/28/1/014204

Photonic crystal fiber polarization filter with two large apertures coated with gold layers

Jun-Jun Wu(吴君君), Shu-Guang Li(李曙光), Qiang Liu(刘强), Min Shi(石敏)
Chin. Phys. B . 2017, 26(11): 114209 . **doi:** 10.1088/1674-1056/26/11/114209

A high figure of merit localized surface plasmon sensor based on a gold nanograting on the top of a gold planar film

Zhang Zu-Yin, Wang Li-Na, Hu Hai-Feng, Li Kang-Wen, Ma Xun-Peng, Song Guo-Feng
Chin. Phys. B . 2013, 22(10): 104213 . **doi:** 10.1088/1674-1056/22/10/104213

Design and optimization of microstructure optical fiber sensor based on bimetal plasmon mode interaction*

Meng Wu(吴萌)[1,2,3], Xin-Yu Liu(刘欣宇)[1,2,3], Gui-Yao Zhou(周桂耀)[1,2,3], Chang-Ming Xia(夏长明)[1,2,3], Bo-Yao Li(李波瑶)[1,2,3], and Zhi-Yun Hou(侯峙云)[1,2,3,†]

[1] *Guangzhou Key Laboratory for Special Fiber Photonic Devices, South China Normal University (SCNU), Guangzhou* 510006, *China*
[2] *Guangdong Province Key Laboratory of Nano-photonic Functional Materials and Devices, South China Normal University, Guangzhou* 510006, *China*
[3] *Guangdong Provincial Engineering Technology Research Center for Microstructured Functional Fibers and Devices, South China Normal University, Guangzhou* 510006, *China*

(Received 12 July 2019; revised manuscript received 10 September 2019; published online 22 November 2019)

A surface plasmon resonance (SPR) sensor with two orthogonal open loops based on microstructured optical fibers (MOFs) is introduced. The interaction between core mode and surface plasmon polariton (SPP) mode produced by two different metal films is studied. Full vector finite element method is used to analyze the coupling and sensing characteristics. The results show that there are three loss peaks near the Au/Ag film, and multi-peak calibration is achieved. Because of the positive and negative sensitivity of the amplitude, the sensor has strong anti-interference capability when the external environment changes. The sensor can detect the refractive index between 1.37 and 1.40, and the working wavelength is between 1600 nm and 2400 nm. Because the sensor has some excellent characteristics, it can be used in biochemical sensing, environmental detection, and other related fields.

Keywords: surface plasma, biosensor, multi-component detection, photonic crystal fiber

PACS: 42.81.Cn, 87.85.fk, 71.45.Gm **DOI:** 10.1088/1674-1056/ab4d48

1. Introduction

Surface plasmons are a coupling of electromagnetic oscillations generated by electromagnetic waves and free electrons at the interface between metal and dielectrics.[1] Due to the sensitivity of surface plasma to the surrounding refractive index, the surface plasmon resonance (SPR)-based optical sensing of several quantities such as chemical, temperature, pressure, force, environmental monitoring, optical fluidic detection, food safety, and biological species have proved to be advantageous.[2] Because the SPR-based technology can implement the promising and powerful optical detection of such as its high sensitivity, real-time sensing, and unmarked biomolecules, SPR has been used to study many different biomedical applications.[3–5] With the development of miniaturized devices based on optical fibers, the shortcomings of traditional devices have been overcome. The SPR-based fiber optic plasmonic sensors (FOPS) have been very attractive for miniaturized sensors.[6] Therefore, it is necessary to develop excellent new biochemical sensors in the FOPS field.

A lot of researches on SPR-based fiber sensors have been reported. In 2017, Rifat *et al.* reviewed photonic crystal fiber sensors based on surface plasmon and reported multifunctional optical fiber sensors.[7] A novel sensing method for simultaneous measurement of seawater temperature and salinity through using C-type micro structured optical fibers was proposed by Zhao *et al.* in 2018.[8] Zhang *et al.* measured hydrogen peroxide and glucose concentrations by using an SPR sensor with a corrosive plasma nanocoating on tilt fiber Bragg grafting.[9] Yang *et al.* proposed a highly sensitive hollow fiber temperature liquid filling sensor based on surface plasmon resonance.[10] Zhao *et al.* proposed a surface plasmon resonance sensor based on concave photonic crystal fibers for low refractive index detection in 2019.[11] We have found the application of FOPS in medical diagnosis, but it is still difficult to identify specific molecules in molecular groups.[6] With the development of SPR technology, the interface between metal and dielectric film could be deposited on the surface of optical fibers.[12] However, in these studies only the SPR effect of a single precious metal was used to explore the change in refractive index. Considering different plasma bands of different metals, multiple signal peaks can be generated during detection to achieve multi-peaks sensing.

Therefore, in the present study, a novel dual-channel sensor is designed based on the flexible characteristics of PCF structure, different plasma bands for Au/Ag, and the necessity of multi-component detection. Owing to the unique structure of the micro structured optical fiber, the sensor can realize online detection. The sensor has a unique structure and can real-

*Project supported by the National Natural Science Foundation of China (Grant Nos. 61575066, 61527822, and 61735005), the Natural Science Foundation of Guangdong Province, China (Grant No. 2017A030313333), the Science and Technology Program of Guangzhou City, China (Grant No. 201707010133), the Science and Technology Planning Project of Guangdong Province, China (Grant No. 2017KZ010201), the GDUPS (2017), the Innovation Project of Graduate School of South China Normal University (Grant No. 2018LKXM040), and the SCNU Study Abroad Program for Elite Postgraduate Students, China.

†Corresponding author. E-mail: houzhiyun@163.com

© 2019 Chinese Physical Society and IOP Publishing Ltd

ize on-line detection. The numerical results show that the core mode in PCF sensor is affected by the SPR at the Au/Ag interface simultaneously, which makes it possible to monitor multiple substances near the Au/Ag films. Meanwhile, the detection of the positive and negative amplitude sensitivity makes the sensor detection stable and also make certain external disturbances eliminated. The unique open-loop structure can be designed according to the specific molecular size, allowing the specific size of molecules to enter into the structure. These excellent sensing characteristics are of great significance for the applications in environmental monitoring, biochemical sensing, *etc*. And Our theoretical research has integrated correct theoretical simulation methods for the design of optical fiber sensors.

2. Structure and basic theory

According to the different plasma wave bands of different metals and polarization demodulation, the sensor was designed as shown in Fig. 1. We designed two open rings and coated Au/Ag films in the vertical and horizontal directions of the microstructured optical fiber, respectively. In the figure, t_u and t_g are the thickness of Au and Ag, respectively, d_u is the diameter of the micro-opening in the vertical analyte channel, d_g the diameter of the micro-opening in the vertical analyte channel, and p the distance between adjacent air holes. The diameters d_g and d_u are $1.2p$ and p, respectively. In order to make the surface plasma mode generated by the silver film fully coupled with the core mode, the air hole size in the x direction near the core is selected to be $0.3p$, and the air aperture size in the y direction near the core is $0.45p$. To maintain the characteristics of the single mode transmission of the designed sensor, and take the flexible adjustability of the PCF structure into account, we chose the size of the cladding holes to be $0.45p$. The device is fabricated by a general stack and draw method.[13] As for the polishing of the side-face MOF, the common method, *i.e*., the optical fiber grinding, such as a very common femtosecond laser or mechanical grinding method can be taken. The metal films can be coated by magnetron sputtering, which is a common method for metal coating.[14]

The dispersion relationship of silica can be described by the well-known Sellmeier equation.[15] The dispersion relation between gold and silver can be described by Drude–Lorentz model.[16,17] Because the guided loss of the guided mode also greatly influences the signal extraction of the sensor, the limiting loss in the x direction and y direction of the guided mode can be expressed by the following formula:

$$L = 8.686 \times \frac{2\pi}{\lambda} \mathrm{Im}(n_{\mathrm{eff}}) \times 10^4, \tag{1}$$

where $\mathrm{Im}(n_{\mathrm{eff}})$ represents the imaginary part of the effective refractive index, and the unit of limiting loss is dB/cm.

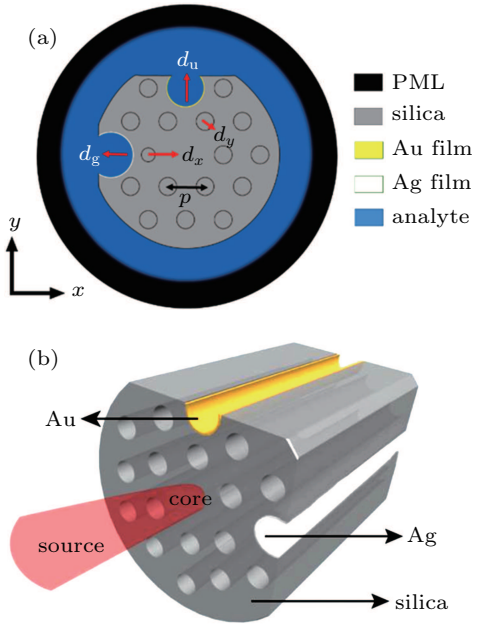


Fig. 1. Schematics of proposed MOF-SPR sensor, showing (a) its cross-section and (b) three-dimensional schematics.

3. Model and theory

In the paper, a full-vector finite-element method is used to calculate the PCF sensor. Firstly, in order to detect the sample signal, we analyze the distribution of modal energy changes in the sample when the refractive index is 1.37 (as shown in Fig. 2), showing that the analysis is in accord with the mode coupling theory that the completely coupling occurs on the sample surface.[18]

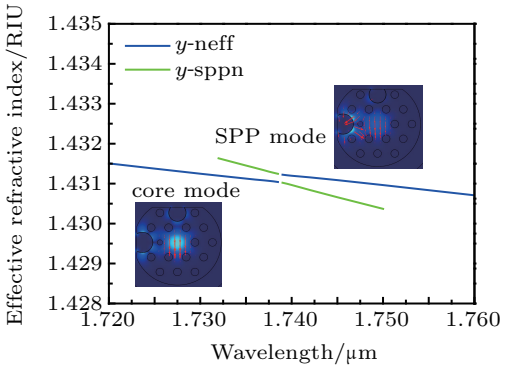


Fig. 2. Reversely crossed plots of effective refractive index *versus* wavelength.

With the refractive index of the external environment changing, the coupling conditions of core mode and SPP mode will vary due to the sensitivity of SPP mode. And the high loss peak will also change. This property can be applied to the sensor device. Hence, we analyze the loss of the y polarized mode when the refractive index of analyte varies from 1.37 to 1.4 (see Fig. 3). Obviously, as the refractive index increases, the loss peak of the y polarized core mode shifts to the longer wavelength in Fig. 3(a). Multiple peak losses occur in the y direction. At the same time, a new sub-peak appears after the first loss peak has vanished. Further analysis of its

energy distribution reveals that the y polarized core mode is affected by SPP mode generated on the Au film and Ag film simultaneously, resulting in another increase of the loss curve that should have decreased, thereby increasing the number of signal peaks. Then the three peaks are fitted, and the results are shown in Figs. 3(b)–3(d).

The sensitivity of the first peak is 409.5 nm/RIU and expressed as ΔP_1. The sensitivity of the second peak is 1550 nm/RIU and expressed as ΔP_2, and the sensitivity of the third peak is 4240 nm/RIU and denoted as ΔP_3. The change of the analyte's refractive index for the y-polarized core mode can be defined as

$$\Delta n = \frac{L_1 \cdot \Delta P_1 + L_2 \cdot \Delta P_2 + L_3 \cdot \Delta P_3}{3},$$

where L_1, L_2, and L_3 represent the variations of the wavelength with their peak change, respectively. We have compared the sensitivities of our proposed optical fiber sensor with those of existing sensors as shown in Table 1.

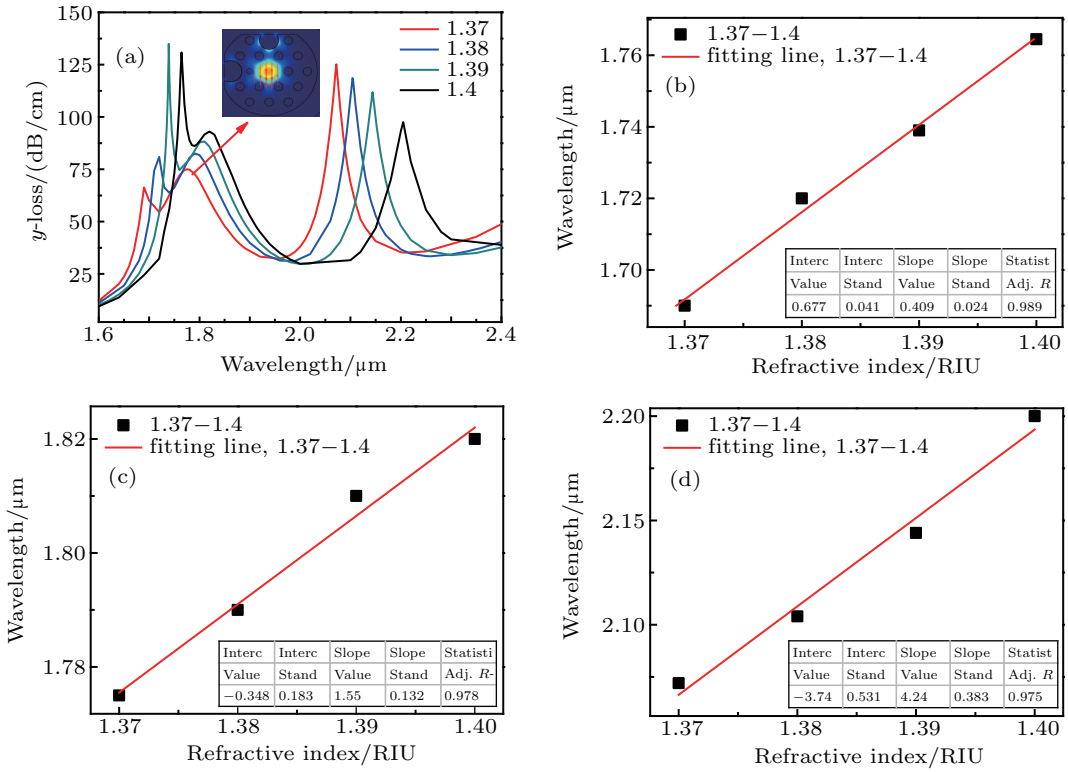


Fig. 3. Sensing properties of y-polarized core mode, showing (a) multi-peak shift to long waveband with refractive index of the analyte increasing, variation of resonance wavelength of (b) the first peak, (c) the second peak, and (d) the third peak with effective refractive index.

Table 1. Comparison of sensitivity between our results and other results from available literature.

Authors	Range of RIU	Sensitivity/(nm/RIU)
Zhen-Kai Fan *et al.*[19]	1.40 to 1.43	3978
Rahul Kumar Gangwar *et al.*[20]	1.43 to 1.46	7700
Rifat *et al.*[21]	1.33 to 1.36	1000
Our work	1.37 to 1.40	4240

Since the film is coated in both directions, the x-polarized core mode will inevitably produce a similar phenomenon that the SPR coupling conditions change with the external analysis fluid. Considering that, we also analyzed the refractive index increasing from 1.37 to 1.41. Figure 4 shows that the loss of x-polarized core mode shifts to longer wavelengths as the refractive index increases. According to equation $S(\lambda) = \Delta\lambda_{\text{peak}}/\Delta n_{\text{a}}$, the slope of sensitivity's fitting curve can be acquired.

Figure 5 shows that the sensitivity of the sensor can reach 4990 nm/RIU. From the fitting results, we can find that the refractive index becomes higher as the wavelength of the x-polarized mode shift grows faster and the linear correlation decreases. It can be explained as the fact that when the sensitive waveband is located around 2 μm, the gold film in the y-direction starts to react at the same time, and the loss change naturally becomes nonlinear.

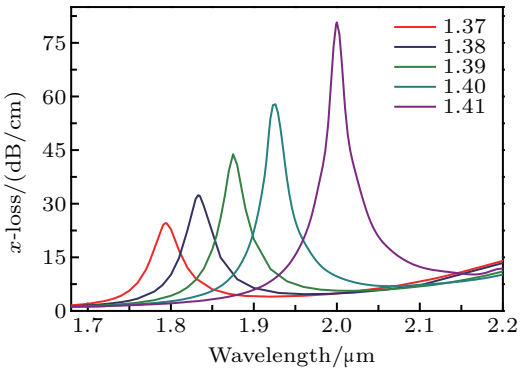


Fig. 4. Plots of loss of x-polarized core mode *versus* wavelength for different indices of analyte.

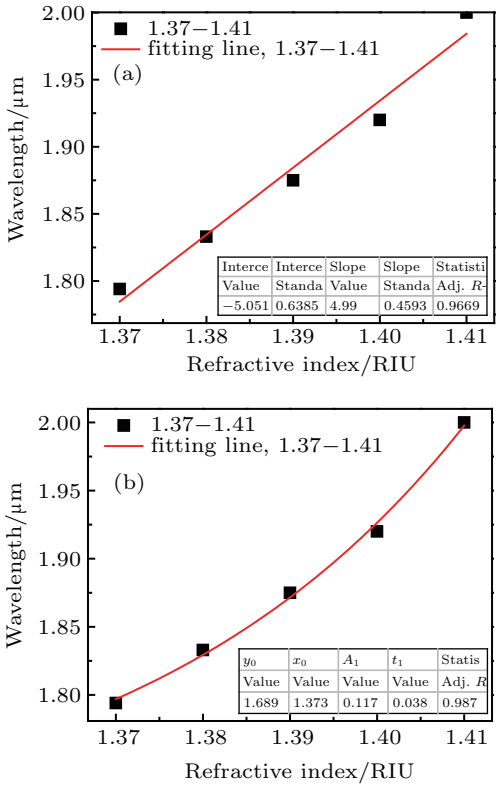


Fig. 5. (a) linear and (b) nonlinear fittings of wavelength *versus* refractive index.

To more accurately describe the change in refractive index, we apply an exponential fit to a nonlinear fitting as shown in Fig. 5(a). Obviously, the fitting coefficient is improved, and the final fitting formula is $Y = y_0 + A_1 \cdot \exp((x - x_0)/t_1)$. The corresponding coefficients are given in the inset of Fig. 5(b). Similarly, the refractive index from the change of the *x*-polarized core mode can be expressed as

$$\Delta(n_1) = (Y + W)/2.$$

Furthermore, we can use the polarization demodulation method to evaluate the change of the refractive index from the *x* and *y* directions. When the light enters into the polarization controller through the 3-dB coupler, it becomes the *x*-direction polarized light, and then it enters into the designed sensor. Afterward, the signal light goes out of the other end of the 3-dB coupler and ultimately enters into the optical spectrum analyzer (OSA) to gain the signal of *x*-polarized core mode. Second, the polarization controller is controlled to obtain the polarized light in the *y* direction entering into the sensor, and the signal is collected by a spectrometer to obtain the signal of *y*-polarized core mode. Finally, the signals in the *x* and *y* directions can be processed according to the following formula: $\Delta n = (\Delta n_1 + \Delta n_2)/2$, where Δn_1 and Δn_2 represent the refractive index changes of the *x*- and *y*-polarized core modes, respectively, and the average refractive index changes are also calculated.

Overall, the third peak's amplitude of *y*-polarized core mode gradually decreases while the signal of *x*-polarized core mode presents positive growth, and we analyze the amplitude sensitivities of these two signal peaks as shown in Fig. 6. According to the sensing setup mentioned above, we can collect the two orthogonal signals by OSA. Owing to the negative and positive amplitude sensitivity of *y*-polarized and *x*-polarized core modes, it can eliminate the external interference and further improve the stability of this system.

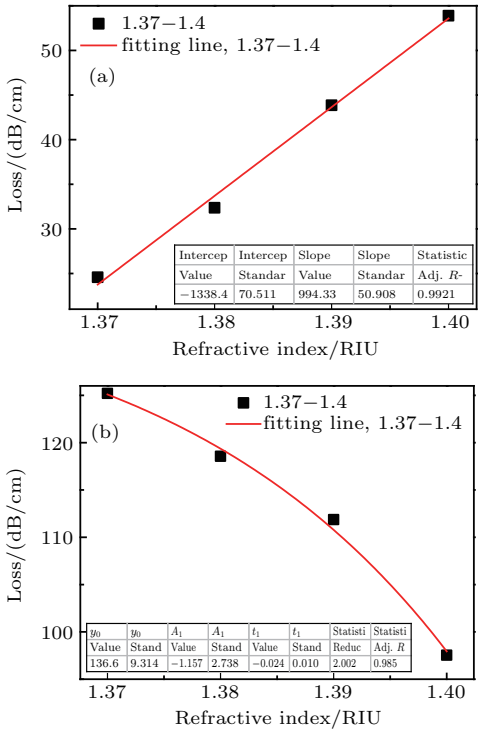


Fig. 6. (a) Linear and (b) nonlinear fitting of loss *versus* refractive index in a range from 1.37 to 1.4.

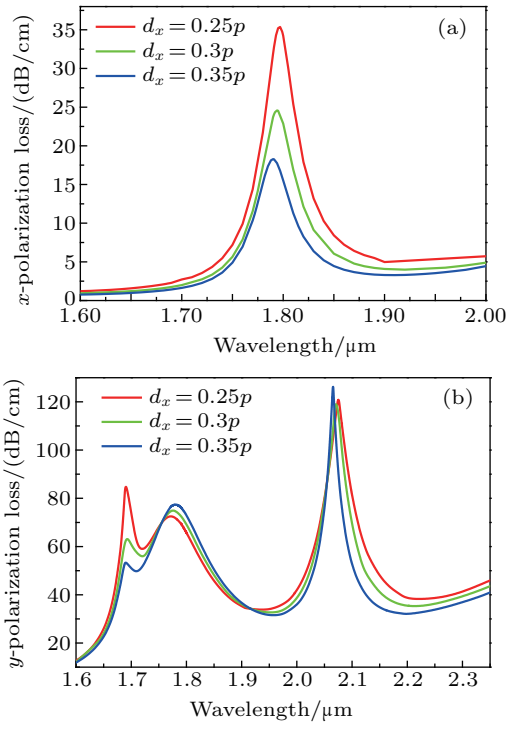


Fig. 7. Variations of (a) *x*-polarization loss and (b) *y*-polarization loss with wavelength for three different values of d_x.

In view of the manufacturing process, we analyze the influence of structural parameters on sensing characteristics. Since the air holes in the x direction near the core are relatively small and easily collapse during drawing, the change in x and y sensing characteristics are shown in Fig. 7 when d_x is $0.25p$, $0.3p$, and $0.35p$, separately.

In Fig. 7, it can be clearly observed that the loss peak of the x-polarized mode does not shift with d_x value increasing. It demonstrates that the change of d_x has little effect on sensing characteristics of the x-polarized mode as the loss becomes larger.

This phenomenon can be easily explained from the analysis of the cross-section of this structure. When the d_x value becomes smaller, the restriction capability of the core for the x-polarized core mode decreases, and the x-polarized core mode is more easily coupled with the SPP mode on silver film, so the loss becomes larger. In addition, the wavelength of the y-polarized core mode does not shift when the d_x value becomes small. However, the loss in the vicinity of 1.7 μm becomes larger. The reason is that the core mode is affected by SPP mode not only on Au but also on Ag due to the decrease of dx value, then the loss becomes larger. Like Fig. 7, figure 8(a) shows the changes of confined loss with d_y. In the shortwave range, the loss peak has almost no shift because the x-polarized core mode is affected by Ag and also by d_y near Au; the loss curve of x-polarized core mode is almost not affected. By contrast, the sub-peak in Fig. 8(b) is influenced by Au, so the loss of y-polarized core mode changes with the variation of d_y.

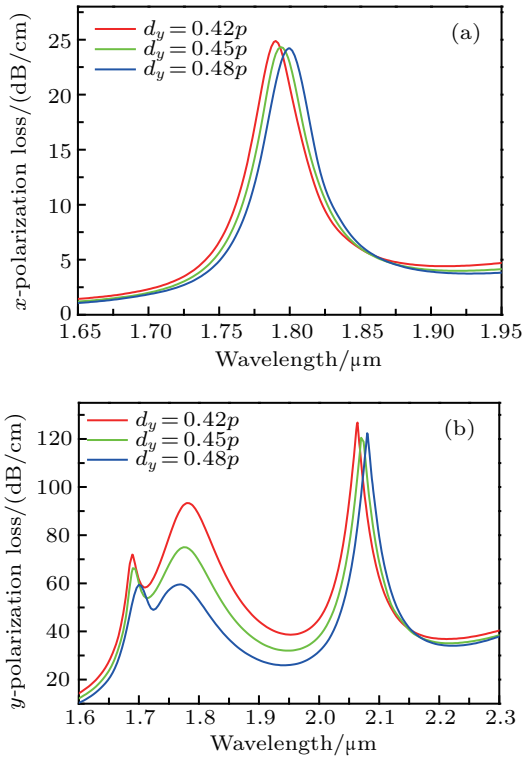


Fig. 8. Variations of (a) x-polarization loss and (b) y-polarization loss with wavelength for different values of d_y.

Considering the influence of pressure in drawing process, we analyze the sensing characteristic changes when d_a value varies from $0.44p$ to $0.45p$ as shown in Fig. 9. It can be found that the loss peak has almost no shift in the shortwave range, but there is a small shift of the loss peak in the long wave range. The period of the air holes is longer than the light wavelength at the shorter wavelength, so the change of the light wave characteristics caused by the slight change of the light wave to the whole cycle is not very clear.

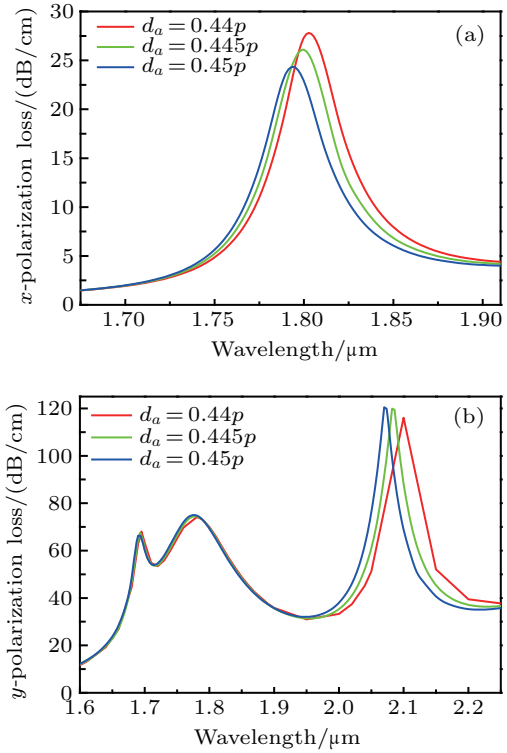


Fig. 9. Variations of (a) x-polarization loss and (b) y-polarization loss with wavelength for different values of d_a.

However, in the long wavelength range, the wavelength is comparable to the periodic size of the crystal structure. Therefore, the changes easily affect the coupling condition between the core mode and the SPP mode, which leads the high loss peak to change.

In addition, the thickness of the gold and silver coating is one of the most important factors that must be considered due to the limit of the actual coating process, thus we explore the changes of the silver film. As shown in Fig. 10, the sensor's sensing characteristics change with the value of t. When the thickness of the film is 40 nm, a sub-peak appears in the y direction, and the coupling effects of gold and silver in both directions are more obvious. It can be concluded that the optimal thickness of the gold film is 40 nm, and the plasmon resonance is the most remarkable.

Now, comes a question: why can a multi-peak effect occur? We study the loss of the y-polarized core mode at longer wavelengths as shown in Figs. 11(a) and 11(b). Comparing

this model, we find that Ag alone produces significant high-loss signal peaks respectively at 1690 nm and 2180 nm for the *y*-polarized core mode, while no high-loss signal peak appears at 1780 nm. In contrast, in the case of a single coating of the Au film, the *y*-polarized core mode has a high loss signal peak at 1780 nm. Therefore, we can confirm that the high-loss signal peaks of the *y*-polarized mode of the proposed sensor are caused by SPP mode generated by Ag film and Au film. How about the characteristic of the *x*-polarization mode? Here in this paper, the effects of separate Au and Ag films on the *x*-polarization core mode with Ag film and Au film are compared with each other (see Figs. 11(c) and 11(d)). In the case of only the Ag film, the *x*-polarized mode produces a high loss peak at 1800 nm and the signal peaks associated well with Au/Ag, while in the case of only the Au, the *x*-polarized mode appears only around 2280 nm. The apparent high loss range also explains that there is a high loss region near 2280 nm under the combined action of Au and Ag.

In summary, the signal peaks of the sensor are from the coupling interaction of core mode and SPP mode generated by Ag film and Au film simultaneously.

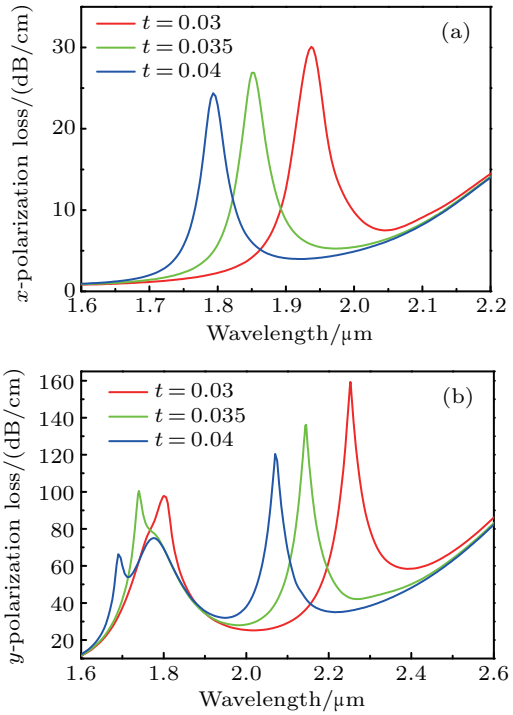


Fig. 10. Variations of (a) *x*-polarization loss and (b) *y*-polarization loss with wavelength at analytical solution's refractive index of 1.37 for different values of *t*.

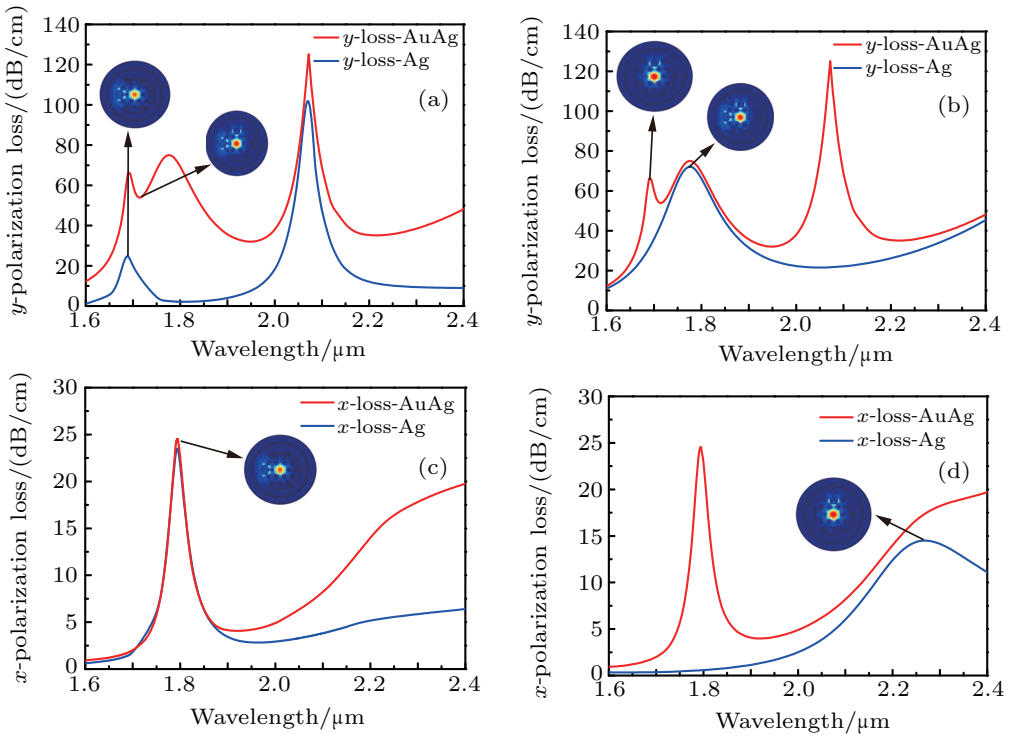


Fig. 11. Comparison between only one metal coated films and Au & Ag coated films, showing variations of *y*-polarization loss with wave length of (a) only Ag-coated film and (b) only Au-coated film, and variations of *x*-polarizaton loss with wavelength of (c) only Ag-coated film and (d) only Au-coated film.

4. Conclusions

In this paper, we present a sensor based on the multi-component detection of gold and silver SPR. The numerical studies reveal that high-loss multi-peaks vary with the refractive index appearing in different wavebands. The larger the phase difference, the stronger the resonance becomes. When the refractive index of the analyte increases from 1.37 to 1.4, the multimode sensitivity of the *y*-polarized core axis is 409.5 nm/RIU, 1550 nm/RIU, and 4240 nm/RIU, respectively. Furthermore, due to the special structure of the device, the two open-loop structures of the sensor can be designed and applied to the relevant biological experimental fields. The study

of bimetallic SPR proves that the orthogonal bimetallic resonance can produce a multimodal effect. At the same time, due to the combined action of Au/Ag, the sensitivities of positive and negative amplitude in x and y directions greatly improve the ability of the sensor to resist external interference. The positive and negative amplitude sensitivity of y-polarized mode makes the sensor detection more stable and some interferences caused by other factors eliminated. Therefore, polarization demodulation technology can be used to measure the concentration of biological liquid more accurately. Through the investigation of the structural characteristics of the proposed sensor, we can find that the sensor has a good structural fault tolerance in practical fabrication. These excellent sensing properties indicate that the sensor has potential application prospects in the fields of drug, food safety, and other biosensors.

References

[1] Brolo A G 2012 *Nat. Photon.* **6** 709

[2] Aruna Gandhi M S, Chu S, Senthilnathan K, Babu P R, Nakkeeran K and Li Q 2019 *Appl. Sci.* **9** 949

[3] Rifat A A, Mahdiraji G A, Sua Y M, Ahmed R, Shee Y G and Adikan F R M 2016 *Opt. Express* **24** 2485

[4] Carrascosa L G, Sina A A I, Palanisamy R, Sepulveda B, Otte M A, Rauf S, Shiddiky M J A and Trau M 2014 *Chem. Commun.* (Camb.) **50** 3585

[5] Polley N, Basak S, Hass R and Pacholski C 2019 *Biosens. Bioelectron.* **132** 368

[6] Guerreiro A, Santos D F and Baptista J M 2019 *Sensors* **19** 1772

[7] Rifat A A, Ahme R, Yetisen A K, Butt H, Sabouri A, Mahdiraji G A, Yun S H and Adikan F R M 2017 *Sens. Actuators B-Chem.* **243** 311

[8] Zhao Y, Peng Y, Chen M Q, Tonga R J 2018 *Sens. Actuators B-Chem.* **263** 822

[9] Zhang X J, Wu Z, Liu F, Fu Q Q, Chen X Y, Xu J, Zhang Z C, Huang Y Y, Tang Y, Guo T and Albert J 2018 *Biomed. Opt. Express* **9** 1735

[10] Yang X C, Lu Y, Liu B L and Yao J Q 2017 *IEEE Photon. J.* **10** 1

[11] Yang Z, Xia L, Li C, Chen X and Liu D M 2019 *Opt. Commun.* **430** 195

[12] Gao S, Chen S S and Lu Q H 2019 *Langmuir* **35** 1040

[13] Chillcce E F, Cordeiro C M B, Barbosa L C and Brito Cruz C H 2006 *J. Non-Cryst. Solids* **352** 3423

[14] Li B Y, Sheng Z C, Wu M, Liu X Y, Zhou G Y, Liu J T, Hou Z Y and Xia C M 2018 *Opt. Lett.* **43** 5070

[15] Xia Y, Zhang Y, Pan S, Shum P, Yan M, Leviatan Y and Li C 2010 *J. Opt.* **12** 015005

[16] Lee H, Schmidt M, Tyagi H, Sempere L and Russell P 2008 *Appl. Phys. Lett.* **93** 111102

[17] Rioux D, Vallières S, Besner S, Muñoz P, Mazur E and Meunier M 2014 *Adv. Opt. Mater.* **2** 176

[18] Han Y H, Xia L X and Liu D M 2014 *Chin. Phys. B* **23** 104219

[19] Fan Z K, Fang S B, Li S G and Wei Z Y 2019 *Chin. Phys. B* **28** 094209

[20] Gangwar R K and Singh V K 2017 *Optik* **12** 1367

[21] Rifat A A, Mahdiraji G A, Shee Y G, Shawon M J and Mahamd Adikan F R 2016 *Procedia Eng.* **140** 1